

Strain-driven self-rolling mechanism for anomalous coiling of multilayer nanohelices

L. Dai and W. Z. Shen^{a)}

Department of Physics, Laboratory of Condensed Matter Spectroscopy and Opto-Electronic Physics, and Key Laboratory of Artificial Structures and Quantum Control, Ministry of Education, Shanghai Jiao Tong University, 1954 Hua Shan Road, Shanghai 200030, China

(Received 30 September 2009; accepted 2 November 2009; published online 9 December 2009)

We have proposed a comprehensive model based on a Cosserat curve to investigate the strain-driven self-rolling mechanism for anomalous coiling of multilayer nanohelices from the biaxial-torque point of view. Special attention has been paid to the edge effects, which dominate the anomalous coiling and decrease the helicity angles to as small as 0. By quantitatively explaining the experiments, we have demonstrated that the edge effects not only generate the torsion torque, together with the initial stress perpendicular to the preferential winding direction, to turn the nanobelts, but also offset part of the initial uniaxial bent torque. Our derived expressions can be used experimentally to determine the geometry of multilayer nanohelices with all helicity angles. The present work has provided useful information for the future experimental investigation on multilayer nanohelices as well as their application in meta-/quantum-devices. © 2009 American Institute of Physics. [doi:10.1063/1.3267866]

I. INTRODUCTION

Nanostructures offer many opportunities for the assembly of nanoscale devices and arrays with potential application in engineering, electronics, electromechanics, and optics.¹⁻⁵ Since Prinz *et al.*⁶ fabricated the InGaAs/GaAs nanotubes and nanohelices based on a strain-driven self-rolling mechanism, the method combining of “top-down” and “self-organization” has been extended to make more complex multilayered hybrid structures composed of metal, dielectric, and magnetic-material layers as well as semiconductor heterostructures.⁷⁻¹³ Nanohelices, used as springs, inductors, sensors, and actuators, constitute a broad and active research field in the micro-/nanoelectromechanical systems (MEMS/NEMS) due to their unique superelasticity behavior¹⁴⁻¹⁷ and piezoresistive, piezoelectric effects.¹⁸⁻²⁰

Generally, the multilayer films persist rolling along the preferential winding direction determined by the orientation of the smallest Young’s modulus, and form the helices with the helicity angles not less than 45° under the uniaxial bent torque induced by the initial stress partially relaxing along the rolled-up direction.¹¹ To make best use of nanohelices in MEMS or NEMS, it is necessary to decrease the helicity angles adequately to leave enough room for deformation. This desirable concept has been materialized in the SiGe/Si and SiGe/Si/Cr nanohelices due to the additional torque coming from the edge effects of stress relaxation at the sides of the nanobelts.²¹ The existed closed-form theories,²²⁻²⁵ however, failed in presenting an accurate description of the strain-driven self-rolling mechanism of nanobelts under the biaxial torque and therefore the geometry of the formed

nanohelices, though they can estimate the curvature radius and strain components of the rolled nanohelices in the uniaxial stress relaxation condition.

In this paper, we establish a theory for exploring the biaxial-torque-drive mechanism of the nanohelices made up from multilayer structures by employing the concept of the extensible and shearable Cosserat curve.²⁶ We not only explain the experimental observation in the literature,^{6-12,21,27} but also demonstrate that the essence of edge effects lies in the capability of bringing a torsion torque to turn the nanobelts and offsetting part of the initial uniaxial bent torque. We have also discussed the effect of the edge effects on the diameters of nanohelices with infinitesimal helicity angles and the relative stretch of nanobelts.

II. THE MECHANICAL CURVE MODEL

The concept of the Cosserat curve was introduced by Cosserat *et al.*²⁸ for a directed curve with an orthonormal triad of directors and specified by four vector fields. Whithman and DeSilva²⁶ further developed the theory of the curve as a special case of the nonlinear, dynamical theory of elastic directed curves and gave the basic equilibrium equations

$$\hat{\tau}_\alpha - \varepsilon_{\alpha\beta\gamma} \tau_\beta W_\gamma = 0, \quad (1a)$$

$$\hat{m}_\alpha - \varepsilon_{\alpha\beta\gamma} (m_\beta W_\gamma + \tau_{\beta\gamma}) = 0, \quad (1b)$$

where τ and m are the total force and torque across the cross section of the curve, respectively, ε is the permutation tensor, W and y are the director and position deformation measure, respectively. The Greek subscripts α , β , and γ take on the values 1, 2, and 3. $(\hat{\cdot}) = \partial/\partial S = \lambda(\dot{\cdot}) = \lambda \partial/\partial s$ and $\lambda = \partial s/\partial S$ is the stretch of the curve with S the arc length along a fixed reference configuration and s the one along a deformed configuration.

^{a)} Author to whom correspondence should be addressed. Electronic mail: wzshen@sjtu.edu.cn.

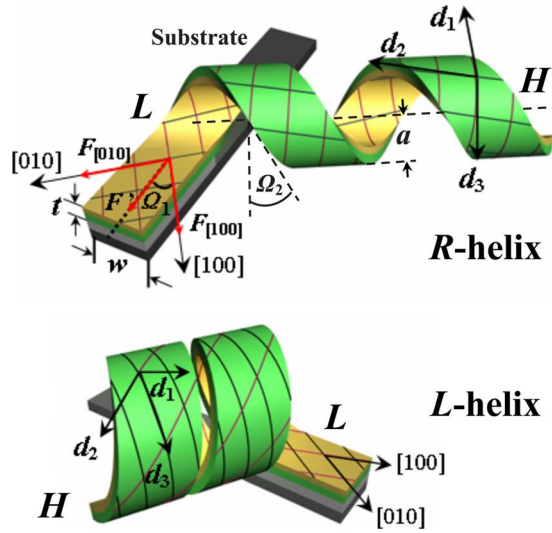


FIG. 1. (Color online) Configuration of the nanohelices H rolled-up from the multilayer nanobelts L . The chirality is determined by the competition between the initial biaxial stress and the edge effects.

As shown in Fig. 1, to establish the Cosserat curve model for exploring exactly the three-dimensional helices formed from the strained multilayer nanobelts, we suppose that a multilayer nanobelt L with a width w and thickness t ($w > t$) is fixed at one end to a substrate, e.g., Si(001), and has misalignment angle Ω_1 degrees from [100]. After the wet etching, the nanobelt L detaches from the substrate and releases the internal strain to form a helix H with a radius a and helicity angle Ω_2 . Its chirality is determined by the competition among the initial biaxial stress $F_{[100]}$, $F_{[010]}$ along [100], [010] directions, and a force F' along the longitudinal axis of the nanobelt, which are induced from the stress relaxation in $\langle 100 \rangle$ and at the sides of the nanobelt, respectively.²¹ In this case, due to the cubic symmetry of the semiconductor [100] is the preferential winding direction for the right-handed helix, named as R-helix, while [010] is the one for the left-handed helix, named as L-helix. Since a line along the preferential winding direction, the black or red one on the nanobelt displayed in Fig. 1, lies in the cylindrical plat of the helix H , it also forms a helix H' with a radius a' and helicity angle Ω_3 . Thus the helix H' can be regarded as a helix rolled from a nanobelt L' along the preferential winding direction with a rectangle cross section of width w' , and thickness t , where for the R-helix $w' = w / \cos \Omega_1$ and for the L-helix $w' = w / \sin \Omega_1$.

In order to give an appropriate description of the rolling behavior for the multilayer nanobelts, we study H' in the Cosserat curve model. The geometry parameters of the helix H can be got from those of the helix H' through the transform relation:

$$a = a', \quad \Omega_2 = |\Omega_1 - \Omega_3|. \quad (2)$$

In this model L' is the fixed reference configuration and H' is the deformed one, whose director basis D_i ($i=1, 2, 3$) and d_i illustrated in Fig. 1 are defined by a set of Euler angles ϕ_0 , θ_0 , and ψ_0 and ϕ , θ , and ψ , respectively.²⁹ For the configuration of helix ϕ_0 , θ_0 , ψ_0 , ϕ , θ , and ψ are all constants,³⁰ the

director deformation measures $W^{(0)}$ of L' and W of H' have the form of

$$W_1^{(0)} = W_2^{(0)} = W_3^{(0)} = 0, \quad (3a)$$

$$W_1 = \hat{\psi} \sin \theta \cos \phi,$$

$$W_2 = \hat{\psi} \sin \theta \sin \phi, \quad W_3 = \hat{\psi} \cos \theta. \quad (3b)$$

We choose the third director D_3 of L' along the tangent to the centerline of the nanobelt axis, and d_1 and d_2 along the direction of the greatest and lowest bending stiffnesses of the cross section in L' , respectively. As a result, the material parameters of d_i are the ones of $\langle 100 \rangle$, which are remain the same due to the cubic symmetry of the semiconductor. For such a case the force and torque in Eq. (1) yields

$$\tau_1 = E_1 y_1, \quad \tau_2 = E_2 y_2, \quad \tau_3 = E_3 (y_3 - 1), \quad (4a)$$

$$m_1 = A W_1, \quad m_2 = B W_2, \quad m_3 = C W_3, \quad (4b)$$

where $E_1 = E_2 = K G t' d$, $E_3 = E t' d$, $A = E I_1$, $B = E I_2$, and $C = G J$. K is the Timoshenko shear coefficients and related to the Poisson's ratio ν through $K = (5 + 5\nu)/(6 + 5\nu)$.³¹ E and $G = E/2(1 + \nu)$ are the equivalent Young's and shear moduli of the nanobelt, respectively.³² $I_1 = w'^3 t / 12$ and $I_2 = w' t^3 / 12$ are the moment of inertia and $J = I_1 + I_2$ is the polar moment of inertia of the cross section.

The force τ is assumed along the e_3 axis of the fixed Cartesian basis. We use that condition in the equilibrium equation Eq. (1b) and obtain

$$B \hat{W}_1 - (B - C) W_2 W_3 - (E_2 - E_3) y_2 y_3 - E_3 y_2 = 0, \quad (5a)$$

$$(A - B) W_1 W_2 = 0. \quad (5b)$$

Since $A \neq B$, Eq. (5b) tells that for a helical solution $W_1 = 0$ or $W_2 = 0$. Taking into account the stability of a helix, $W_1 = 0$ is energetically favored, which suggests that $W_2 = \hat{\psi} \sin \theta$ in Eq. (3b). Through Eq. (4b), the torque obeys the expression with respect to the director deformation measure W

$$m_1 = 0, \quad m_2 = B \hat{\psi} \sin \theta, \quad m_3 = C \hat{\psi} \cos \theta. \quad (6)$$

The position vectors obtained from Eq. (1a) of H_F satisfying $y_1 = 0$, $y_2 = \tau \sin \theta / E_2$, and $y_3 = \tau \cos \theta / E_3 + 1$, from which we can have not only the stretch λ

$$\lambda = \sqrt{\frac{\tau^2}{E_2^2} \sin^2 \theta + \left(\frac{\tau}{E_3} \cos \theta + 1 \right)^2}, \quad (7)$$

but also the radius, pitch, and helicity angle of H' in terms of the Euler angles

$$a' = \frac{1}{\hat{\psi}} \left[\left(\frac{\tau}{E_3} \cos \theta + 1 \right) - \frac{\tau}{E_2} \cos \theta \right] \sin \theta, \quad b' \\ = \frac{2\pi}{\hat{\psi}} \left[\frac{\tau}{E_2} \sin^2 \theta + \left(\frac{\tau}{E_3} \cos \theta + 1 \right) \cos \theta \right],$$

$$\Omega_3 = \arctan(b'/2\pi a'). \quad (8)$$

By virtue of Eqs. (3) and (5a) and the position vectors, the force τ subjects to the constraint

$$\left(\frac{1}{E_3} - \frac{1}{E_2}\right) \cos \theta \tau^2 + \tau + (B - C) \hat{v}^2 \cos \theta = 0. \quad (9)$$

It turns out that with the knowledge of the force τ or the torque m , the radius a' , pitch b' , and the stretch λ of a helix can be derived through Eqs. (6)–(9). Vice versa, when the geometry parameters of a helix are the given physical quantities, those equations also provide us a method to give a picture of the force τ and torque m on the helix. By scanning electron microscope (SEM) observations of the multilayer rolled-up nanostructures, the latter application is very useful for understanding the biaxial-torque characteristics induced from the stress relaxation.

III. CONVENTIONAL SITUATION WITHOUT EDGE EFFECTS

We start the demonstration of the proposed Cosserat curve in the conventional situation, that is, the nanobelt rolls along the preferential winding direction when the stress relaxation at the sides of the nanobelt can be omitted. In such a case, $F_{[100]}$ and $F_{[010]}$ generate two bent torques $M_{[100]}$ and $M_{[010]}$, respectively. It is thought that the initial biaxial stress in the nanobelt is partially relaxed along the rolled-up direction, i.e., a uniaxial bent torque condition, and $m_2 = M_{[100]}$ and $m_3 = 0$ for the chosen director basis of d_i . However, the real multilayer nanostructures suffer the biaxial bent torque (the stress relax in the direction of both preferential rolling and the one perpendicular to it), which leads to another torque along d_3 : $m_3 = M_{[010]} \neq 0$.

For the uniaxial bent torque case, we simulate the experimental results of an R-helix formed from a p -type SiGe/Si bilayer heterofilm of the width $w = 1.3 \mu\text{m}$, layer thickness $t_{\text{SiGe}} = 11 \text{ nm}$, $t_{\text{Si}} = 8 \text{ nm}$, and misalignment angle $\Omega_1 = 50^\circ$.²¹ Following Tsui *et al.*,³³ we have $M_{[100]}$ in the form of

$$M_{[100]} = \frac{F_{[100]} t}{2} \frac{t}{2}, \quad (10)$$

where $F_{[100]} = \varepsilon_{\text{SiGe}} E_{\text{SiGe}} w' t_{\text{SiGe}}$ with $w' = w / \cos \Omega_1$ for [100] and $w' = w / \sin \Omega_1$ for [010]. $\varepsilon_{\text{SiGe}}$ is the lattice mismatch and E_{SiGe} is Young's modulus of SiGe layer. Using Eqs. (2) and (6)–(10) and $m_2 = M_{[100]}$, $m_3 = 0$, we can fit both the SEM observations of the helicity angle Ω_2 of 50° and the diameter of the helix of $1.26 \mu\text{m}$, with the geometry parameters of misalignment angle and layer thickness as well as $E_{\text{Si}} = 130.2 \text{ GPa}$, $E_{\text{SiGe}} = 161.2 \text{ GPa}$, and $\varepsilon_{\text{SiGe}} = 1.6\%$.²¹ With further considering the biaxial bent torques of $m_2 = M_{[100]}$ and $m_3 = M_{[010]}$, we find that the helicity angle and diameter almost remain the same as that of the uniaxial stress relaxed condition with the additional material parameters of $\nu_{\text{SiGe}} = \nu_{\text{Si}} = 0.27$.³⁴ It suggests that the bent torque along d_3 is not large enough to drive the nanobelt roll away from the preferential winding direction as most experimental results have shown.^{6–12} Thus by quantitatively explaining the experimen-

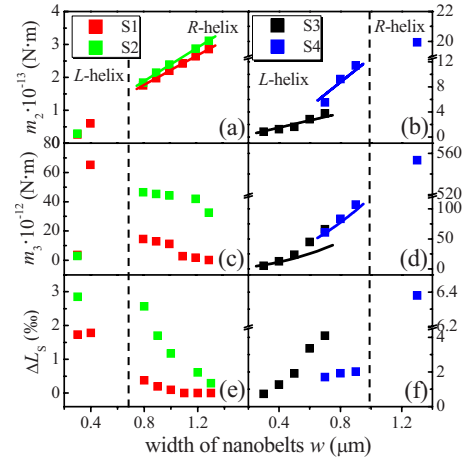


FIG. 2. (Color online) Theoretical calculations (squares) based on the Cosserat curve model of the torque m_2 , m_3 , and the relative stretch ΔL_S vs the width of nanobelts w for [(a), (c), and (e)] S1, S2 and [(b), (d), and (f)] S3, S4, together with the fitting results (lines and curves).

tal observation in the literature, we have demonstrated that, without the edge effects, the nanohelices with helicity angles less than 45° cannot be achieved even though the initial biaxial stress both relaxed as bent torque.

IV. FUNCTION OF THE EDGE EFFECTS

A. Anomalous coiling of nanobelts induced by biaxial torque

The helices with the helicity angles less than 45° result from the relaxation of stress perpendicular to the nanobelts orientation, where the force F' dominates the deviation behavior of the nanobelts. We now concentrate on the biaxial torque induced by the two components along $\langle 100 \rangle$ of F' : $F'_{[100]}$ and $F'_{[010]}$. The component of F' perpendicular to the preferential winding direction turns the nanobelt and generates a torsion torque M_T along d_3 together with the initial stress of the same direction, while the component of F' along the preferential winding direction prevents the other initial stress from driving the nanobelt roll in $\langle 100 \rangle$ and brings a bent torque M_B along d_2 .

As a numerical example, Figs. 2(a)–2(d) present the theoretical calculations (squares) of the torque m_2 and m_3 versus the width of nanobelts w , deduced from Eqs. (5a), (5b), (6), (8), and (9) with the experimental results of diameter and helicity angle, for the four sets of multilayer nanohelices: S1, the SiGe/Si with layer thickness 11/8 nm, $\Omega_1 = 50^\circ$; S2, the SiGe/Si with 11/8 nm, $\Omega_1 = 55^\circ$; S3, the SiGe/Si/Cr with 11/8/10 nm, $\Omega_1 = 50^\circ$; and S4, the SiGe/Si/Cr with 11/8/21 nm, $\Omega_1 = 55^\circ$.²¹ To make an accurate description of the torque, we study the data of the R-helix for S1 and S2, and L-helix for S3 and S4 with the material parameters of Si and SiGe, together with $E_{\text{Cr}} = 377 \text{ GPa}$ and $\nu_{\text{Cr}} = 0.31$.³⁵ As shown in Figs. 2(a) and 2(b), the torque m_2 of both the R-helix and L-helix decreases linearly with the width of nanobelts w .

According to the definition of the bent torque M_B , for the bilayer nanobelts we have

$$M_B = \frac{F_{\langle 100 \rangle} - F'_{\langle 100 \rangle} t}{2} \quad (11)$$

while for the trilayer ones M_B can be expressed as³³

$$M_B = \frac{F_{\langle 100 \rangle} - F'_{\langle 100 \rangle}}{2} \left(\frac{3}{2} t_{Cr} - \delta \right), \quad (12)$$

where $\delta = E_{SiGe} t_{SiGe}^2 - E_{Si} t_{Si}^2 / 2 (E_{SiGe} t_{SiGe} + E_{Si} t_{Si})$ and $F_{\langle 100 \rangle} = (\varepsilon_{SiGe} E_{SiGe} t_{SiGe} + \varepsilon_{Cr} E_{Cr} t_{Cr}) w'$. $\varepsilon_{Cr} = 0.95\%$ is the lattice mismatch of Cr layer.³⁵ Since F' is independent of the width for a given nanobelt, we can use Eqs. (11) and (12) and the relation of $m_2 = M_B$ to fit the theoretical results of the Cosserat curve model, as the curves displayed in Figs. 2(a) and 2(b), and get F' for the three kinds of multilayer nanobelts: $F' = 3.8 \times 10^{-6}$ N for S1 and S2 (average value), $F' = 1.6 \times 10^{-5}$ N for S3, and $F' = 5.6 \times 10^{-5}$ N for S4. Obviously, F' increases with the Cr film thickness, i.e., adding a strained isotropic film will strengthen the effects of stress relaxation at the sides, in good agreement with the experiments.²¹

The torque m_3 has a more complex variation with the width of nanobelts than that of m_2 . It is illustrated in Figs. 2(c) and 2(d) that for the R-helix, the torque m_3 increases with decreasing w , while for the L-helix m_3 varies in the contrary way. We can understand that phenomenon through the torsion torque M_T along d_3 with $M_T = (F_{\langle 100 \rangle} + F'_{\langle 100 \rangle}) r$, where r is the torsion width. In the R-helix, the force F' is not strong enough to turn a rather wide nanobelt, whereas with a decreasing w the force F' makes a rising effect, which broadens the torsion width r to all the width of nanobelt and leads to an increasing m_3 even the initial stress decreases. In the L-helix, because the torsion width r equals to the width of nanobelt, we can estimate m_3 by $m_3 = (F_{\langle 100 \rangle} + F'_{\langle 100 \rangle}) w'$ with the force F' deduced from m_2 . The calculated results (curves) are shown in Fig. 2(d), where in S4 agreement with the data derived from the Cosserat curve model is perfect, while in S3 the surface-stress effects we omitted in M_T are the possible sources of the small deviation.

B. Stretch and nanoring

The particular importance of the Cosserat curve model lies in the ability in deducing the stretch of a nanobelt after it strolls to a helix. In order to make a detailed description of the stretch for a nanobelt, we have further calculated the relative stretch $\Delta L_S = \lambda - 1$ based on Eq. (7). Figures 2(e) and 2(f) display how the relative stretch depends on the width of nanobelts w for the four sets of multilayer nanohelices. It is found that for the nanobelts of different width ΔL_S obeys a similar trend of variation with that of the torque m_3 , i.e., a narrower nanobelt results in a larger stretch in the R-helix and a smaller one in the L-helix. We note that the relative stretch of a helix with helicity angle smaller than 45° is about several thousand percents. Now that a nanobelt has such an amount of stretch without a load, its extension will play a key role in the high-strain region of MEMS/NEMS.

It is well known that with an appropriate small width, a nanobelt oriented away from $\langle 100 \rangle$ can form a ring by scroll-

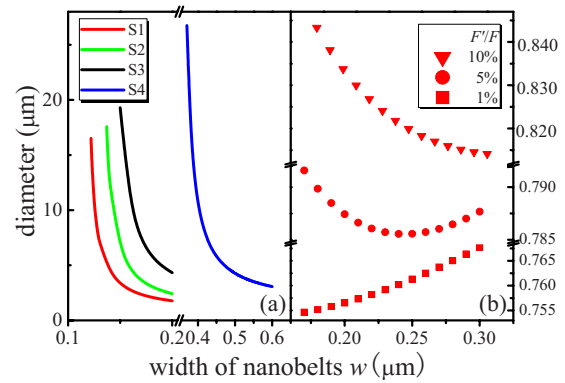


FIG. 3. (Color online) Nanobelt width w dependence of nanoring diameter deduced from the Cosserat curve model for (a) S1-S4 and for (b) a typical nanohelix with the ratio between F' and F equaling to 10%, 5%, and 1%.

ing along its longitudinal axis, and different size rings can be achieved by using nanobelts with further decreasing width. We finally talk about the relation between the width of a nanobelt and the diameter of the formed ring, since the helix with infinitesimal helicity angle has its unique advantages in MEMS/NEMS. Although Zhang *et al.*²¹ have not performed such experiments on the multilayer nanobelts of SiGe/Si and SiGe/Si/Cr, we can investigate theoretically the variation in nanoring size with the nanobelt width based on the established Cosserat curve model. Figure 3(a) presents the diameter of nanorings versus the width of nanobelts w deduced from Eqs. (5a), (5b), and (6)–(9) for S1–S4. For all the four sets of nanorings, their diameters increase significantly with decreasing w to the rather large values, which suggests that F' may offset part of the initial stress F and weaken the rolling behavior of narrow nanobelts. To better understand the joint effect of the two kinds of forces on the geometry of nanorings, we suppose that a typical nanohelix of the same physical parameters as S1 has the ratio between F' and F equaling to 10%, 5%, and 1% as presented in Fig. 3(b). A large F'/F of 10% brings an increasing diameter with the decrease of w , while a small F'/F of 1% leads to a decreasing one (similar experimental results have been reported in Si/Cr nanorings²⁷). Nevertheless, for $F'/F = 5\%$, the diameter no longer monotonously change with w . It is clear that choosing the material with proper F' is helpful to form a self-contact helix in nanoscale. We hope that the present study can stimulate further experimental investigations on the complicated influence of the edge effects on nanohelices geometry.

C. Impact to experiments

Our investigation of the anomalous coiling of multilayer nanohelices provides the experimenters a guide to acquire better growth technology. Although the nanohelices and nanorings with helicity angles less than 45° could be fabricated, the mechanism of the edge effects was still unclear. By quantitatively explaining the experiments, we have demonstrated that the present mechanical curve model can give a detailed analysis of the edge effects, with the aid of the SEM observations of the multilayer rolled-up nanostructures. Most importantly, since the geometry of nanohelices and nanorings

can be foretold with the knowledge of the function of the edge effects according to our model, any morphology of those structures can be designed as the proper materials are chosen. Then a controllable growth process can be achieved for all nanohelices and nanorings of complex multilayered hybrid structures based on strain-driven self-rolling mechanism. Moreover, due to the small sizes and three-dimensional structures of nanohelices and nanorings, it is difficult to get the direct measures for the stretch of nanobelts during the strolling process from experiments. That difficulty can be solved by employing our model to have an accurate evaluation.

V. CONCLUDING REMARKS

In summary, we have elucidated the strain-driven self-rolling mechanism of multilayer nanohelices from the biaxial-torque point of view through proposing the Cosserat curve model. By explaining the experimental observation in the literature, we demonstrate that, without the edge effects, the nanohelices with helicity angles less than 45° cannot be achieved even though the initial biaxial stress both relaxed as bent torque. The edge effects not only generate the torsion torque, together with the initial stress perpendicular to the preferential winding direction, to turn the nanobelts, but also offset part of the initial uniaxial bent torque. A complicated influence is therefore found for the dependence of the diameters of nanohelices with infinitesimal helicity angles on the width of nanobelts. From the relative stretch of nanobelts during the rolling process, it is predicted that the extension of materials will play a key role in the high-strain region. With the knowledge of the biaxial-torque-drive mechanism of multilayer nanohelices, our present work applies a reliable reference for the further design and fabrication of meta-/quantum-devices for the potential applications in MEMS/NEMS.

ACKNOWLEDGMENTS

This work was supported by the Natural Science Foundation of China under Contract No. 10734020 and National Major Basic Research Project of 2006CB921507

¹S. Iijima, *Nature (London)* **354**, 56 (1991).

²Y. Cui and C. M. Lieber, *Science* **291**, 851 (2001).

³O. G. Schmidt and K. Eberl, *Nature (London)* **410**, 168 (2001).

⁴Z. L. Wang, *Nanowires and Nanobelts: Materials, Properties and Devices* (Kluwer/Academic, Boston, 2003).

⁵A. Cho, *Science* **313**, 164 (2006).

⁶V. Y. Prinz, V. A. Seleznev, A. K. Gutakovskiy, A. V. Chehovskiy, V. V. Preobrazhenskii, M. A. Putyato, and T. A. Gavrilova, *Physica E (Amsterdam)* **6**, 828 (2000).

⁷O. G. Schmidt, N. Schmarje, C. Deneke, C. Muller, and N. Y. Jin-Phillipp, *Adv. Mater.* **13**, 756 (2001).

⁸V. Y. Prinz, *Microelectron. Eng.* **69**, 466 (2003).

⁹S. Mendach, O. Schmacher, C. Heyn, S. Schnull, H. Welsch, and W. Hansen, *Physica E (Amsterdam)* **23**, 274 (2004).

¹⁰L. Zhang, E. Deckardt, A. Weber, C. Schonenberger, and D. Grutzmacher, *Nanotechnology* **16**, 655 (2005).

¹¹R. Songmuang, C. Deneke, and O. G. Schmidt, *Appl. Phys. Lett.* **89**, 223109 (2006).

¹²I. S. Chun, V. B. Verma, V. C. Elarde, S. W. Kim, J. M. Zuo, J. J. Coleman, and X. Li, *J. Cryst. Growth* **310**, 2353 (2008).

¹³Y. F. Mei, D. J. Thurmer, C. Deneke, S. Kiravittaya, Y. F. Chen, A. Dadgar, F. Bertram, B. Bastek, A. Krost, J. Christen, T. Reindl, M. Stoffel, E. Coric, and O. G. Schmidt, *ACS Nano* **3**, 1663 (2009).

¹⁴X. Chen, S. Zhang, D. A. Dikin, W. Ding, R. S. Ruoff, L. Pan, and Y. Nakayama, *Nano Lett.* **3**, 1299 (2003).

¹⁵D. J. Bell, L. X. Dong, B. J. Nelson, M. Golling, L. Zhang, and D. Grutzmacher, *Nano Lett.* **6**, 725 (2006).

¹⁶P. X. Gao, W. J. Mai, and Z. L. Wang, *Nano Lett.* **6**, 2536 (2006).

¹⁷C. B. Cao, H. L. Du, Y. J. Xu, H. S. Zhu, T. H. Zhang, and R. Yang, *Adv. Mater.* **20**, 1738 (2008).

¹⁸Y. W. Hsu, S. S. Lu, and P. Z. Chang, *J. Appl. Phys.* **85**, 333 (1999).

¹⁹K. Hjort, J. Soderkvist, and J. A. Schweitz, *J. Micromech. Microeng.* **4**, 1 (1994).

²⁰G. Hwang, H. Hashimoto, D. J. Bell, L. X. Dong, and B. J. Nelson, *Nano Lett.* **9**, 554 (2009).

²¹L. Zhang, E. Ruh, D. Grutzmacher, L. X. Dong, D. J. Bell, B. J. Nelson, and C. Schonenberger, *Nano Lett.* **6**, 1311 (2006).

²²M. Grundmann, *Appl. Phys. Lett.* **83**, 2444 (2003).

²³G. P. Nikishkov, *J. Appl. Phys.* **94**, 5333 (2003).

²⁴J. Zang and F. Liu, *Appl. Phys. Lett.* **92**, 021905 (2008).

²⁵Y. Nishidate and G. P. Nikishkov, *J. Appl. Phys.* **105**, 093536 (2009).

²⁶A. B. Whitman and C. N. DeSilva, *J. Elast.* **4**, 265 (1974).

²⁷L. Zhang, L. X. Dong, D. J. Bell, B. J. Nelson, C. Schonenberger, and D. Grutzmacher, *Microelectron. Eng.* **83**, 1237 (2006).

²⁸E. Cosserat and F. Cosserat, *Theorie des Corps Deformables* (Hermann, Paris, 1909).

²⁹A. E. H. Love, *A Treatise on the Mathematical Theory of Elasticity* (Dover, New York, 1944).

³⁰Z. Zhou, P. Y. Lai, and B. Joós, *Phys. Rev. E* **71**, 052801 (2005).

³¹W. A. Fate, *J. Appl. Phys.* **46**, 2375 (1975).

³²S. P. Timoshenko and J. M. Gere, *Mechanics of Materials* (Van Nostrand, Princeton, 1972).

³³Y. C. Tsui and T. W. Clyne, *Thin Solid Films* **306**, 23 (1997).

³⁴F. Elstner, C. Gautier, O. Piot, G. Contoux, F. Cosset, F. Nardou, and J. Machet, *Phys. Status Solidi A* **154**, 669 (1996).

³⁵S. V. Golod, V. Ya. Prinz, P. Wägli, L. Zhang, O. Kirfel, E. Deckhardt, F. Glaus, C. David, and D. Grützmacher, *Appl. Phys. Lett.* **84**, 3391 (2004).